Comparative Study on Electrical Discharge and Operational Characteristics of Needle and Wire-Cylinder Corona Chargers

Panich Intra* and Nakorn Tippayawong**

Abstract - The electrical discharge and operational characteristics of needle and wire-cylinder corona charger based on current measurements for positive and negative coronas were evaluated and compared. A semi-empirical method was used to determine the ion concentrations in the charging zone and at the outlet of both chargers. Results from experimental investigation revealed that magnitudes of the charging current from the wire-cylinder charger were approximately 3.5 and 2 times smaller than those from the needle charger for the positive and negative coronas, respectively. The ion number concentrations at the outlet for positive corona of both chargers were higher than for negative corona at the same voltage. Flow and electric fields in the charging zone of both chargers were also analyzed via numerical computation. Strong electric field strength zone was identified and led to high charging and particle deposition. Effect of particle deposition on the evolution of discharge current was presented. It was shown that ions loss inside the wire-cylinder charger was higher than the needle charger. The particle deposited on the corona electrodes and on the grounded cylinder caused a great reduction in charging efficiency of both chargers.

Keywords: Electrical discharge, Needle charger, Wire-cylinder charger, Particle deposition

1. Introduction

Corona discharge produces high concentration unipolar ions that are used to produce highly charged aerosols via field- and diffusion-charging mechanisms. It is often necessary to estimate the number of charge on a particle of any given size, based on the conditions under which it acquires the charge. The relationship between the average number of elementary charges and the size of the particles determines their electrical mobility. It is a widely and successfully used technique for aerosol chargers. Both needle and wire-cylinder corona chargers have been utilized and evaluated [1, 2]. However, to our knowledge, no study has been carried out to compare their electrostatic characteristics. This paper presents an attempt to characterize and make comparison between electrical discharge properties of the two chargers.

In this paper, the electrostatic properties in terms of voltage-current relationships of both wire-cylinder and needle corona chargers were compared and discussed for positive and negative coronas in the charging zones. A semi-empirical method, based on ion current measurement and electrostatic charging theory, was used to calculate average ion concentration in the charging zone for each charger [3]. Effect of particle deposition on the evolution of discharge current was presented. A numerical model was employed to describe flow and electric fields in the charging zones to give a better understanding on the operation of the chargers.

* Dept. of Mechanical Engineering, Chiang Mai University, Chiang Mai, 50200 Thailand. (panich_intra@yahoo.com)
** Dept. of Mechanical Engineering, Chiang Mai University, Chiang Mai, 50200 Thailand. (nakorn@dome.eng.cmu.ac.th)
Received December 15, 2005 ; Accepted November 14, 2006

2. Experimentation

The needle and wire-cylinder corona chargers tested in the present study are shown in Fig. 1. The needle charger's geometrical configuration is similar to the charger used by Hernandez-Sierra, *et al.* [2] (Fig. 1a). It consists of a coaxial corona-needle electrode placed along the axis of a cylindrical tube with tapered end. The needle electrode is made of a stainless steel rod, 3 mm in diameter and 49 mm in length, ending in a sharp tip. The angle of the needle cone is about 9^{o} and the tip radius is about 50 μm, as estimated under a microscope. The outer cylindrical is made of an aluminum tube, 30 mm in diameter and 25 mm in length with conical shape. The angle of the cone is about 30^{o} and the orifice diameter is about 4 mm. The distance between the needle electrode and the cone apex is 2 mm. The corona-needle electrode head is connected to an adjustable DC high voltage supply, while the outer electrode is grounded. The wire-cylinder corona charger has a geometrical configuration similar to that used by Keskinen, *et al.* [4] (Fig. 1b). It consists of a coaxial corona-wire electrode placed along the axis of a metallic cylinder tube. The outer cylindrical is made of an

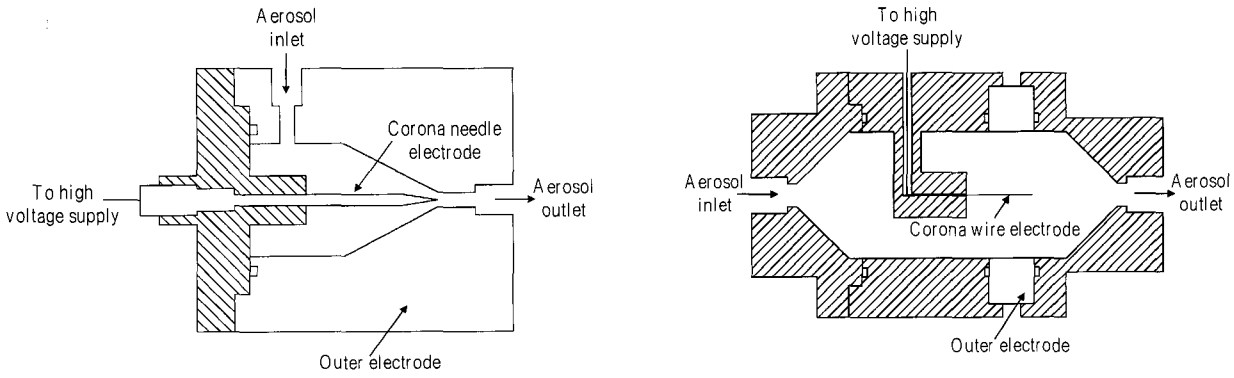

(a) needle (b) wire-cylinder

Fig. 1 Schematic diagrams of the needle and wire-cylinder chargers

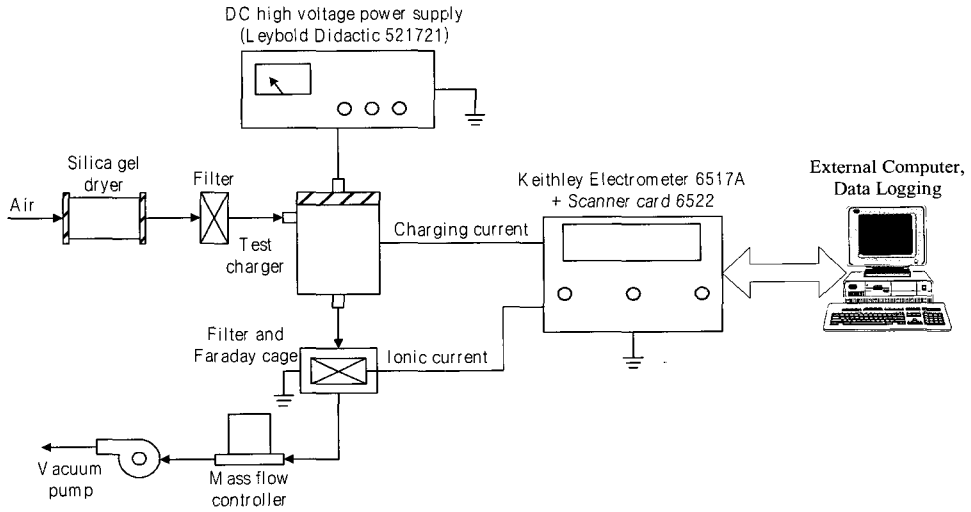

Fig. 2 Experimental setup for electrical discharge characterization

aluminum tube, 28 mm in diameter and 10 mm in length. The wire electrode is made of a stainless steel wire, 300 μm in diameter and 10 mm in length. An adjustable DC high voltage supply is used to produce the corona discharge on the wire electrode while the outer metallic electrode is grounded.

The electrical discharge characterization experiments were carried out using the setup sketched in Fig. 2. Clean dry air flow was regulated and controlled by means of a mass flow meter and controller, typically in the range between 0 – 30 liter/min. The air flow was forced by a vacuum pump. An adjustable DC high voltage power supply (Leybold Didactic model 521721, 500 mV peak-to-peak ripple voltage, and 0.5 mA maximum current) was used to maintain the corona voltage difference, generally in the range between 1-10 kV. The charging current from the corona electrode was measured directly with the sensitive electrometer (Keithley 6517A electrometer incorporating a Keithley 6522 scanner card interfaced to a personal computer via an RS-232 interface) via the outer electrode.

It is desirable to know the ion number concentration within the charging zone, N_i, because the $N_i t$ product is the main parameter controlling the efficiency of particle charging. In this study, the ionic current at the charger outlet was measured by filtration method. An air sample was drawn into a shielded Faraday cage with a filter through which all the air passed. The filter was equipped with a fine collection metal grid, and was electrically isolated from the Faraday cage and ground. High efficiency particulate-free air (HEPA) filter was used for these experiments because the collection efficiency for small air ions was very high. In the Faraday cage, the charges were removed from the air stream by the filter and the resulting ionic current flow was monitored with the sensitive electrometer. Both the charging current and ionic current were recorded by a personal computer and used for calculation of corresponding total ion number concentration.

3. Theory

On the basis of Maxwell's theory, the electric field between the two electrodes of the charger is given by

$$\text{div}\,\vec{E} = \frac{\rho}{\varepsilon_0} \tag{1}$$

where $\vec{E}$ is the electric field, ρ is the space charge density, and ε_0 is the vacuum permittivity. The ion current density, $\vec{j} = \rho\vec{u}_i$ with the mean ionic velocity, $u_i = Z_i E$, where Z_i is the electrical mobility of the ions. The ion current density can be expressed on the basis of the ion current, I_i, through the inner surface area, A, of the outer electrode of the charger as

$$\rho Z_i E = \frac{I_i}{A} \tag{2}$$

The space charge defines in terms of the ion concentration N_i, is $\rho = N_i e$ where e is the elementary charge. Substituting into equation (2), the mean ion number concentration in the charging zone of the charger in the absence of aerosol particles is given by

$$N_i = \frac{I_i}{eZ_i EA} \tag{3}$$

3.1 Ion Concentration in Charging Zone of the Needle Charger

The inner surface area of the metallic cone (charger outlet) where the ion current is collected, and is given by

$$A = \pi(r_1 + r_2)\sqrt{(r_1 - r_2)^2 + L^2} \tag{4}$$

where r_1 and r_2 are the inner and outer radii of a conical frustum, and L is the length of the charging zone. If the space charge effect is neglected, the electric field strength was estimated to be given by the simplified equation

$$E = \frac{V}{d} \tag{5}$$

where V is the applied voltage, and d is the distance between the electrode tip and the cone apex. Substituting equation (4) and equation (5) into equation (3) gives

$$N_i = \frac{I_i d}{\pi(r_1 + r_2)\sqrt{(r_1 - r_2)^2 + L^2}\,eZ_i V} \tag{6}$$

The $N_i t$ product (mean ion number concentration × mean aerosol residence time) is a fundamental parameter to describe the operation of an aerosol charger, because it is intimately related to the extent to which the particles can become charged. The mean aerosol residence time of the particles in the charging zone of the charger is given by

$$t = \frac{\pi L\left(r_1^2 + r_1 r_2 + r_2^2\right)}{3Q_a} \tag{7}$$

where Q_a is the aerosol flow rate. For the standard aerosol flow of 5.0 liter/min, the mean aerosol residence time in the charging zone is 0.0814 s at atmospheric pressure.

3.2 Ion Concentration in Charging Zone of the Wire-Cylinder Charger

The inner surface area of the outer electrode of the charger is given by

$$A = 2\pi rL \tag{8}$$

If the space charge effect is neglected, the electric field, E, in the charging zone is given by Gauss's law,

$$E = \frac{V}{r\ln(r_2/r_1)} \tag{9}$$

where r_1 and r_2 are radii of the inner and outer electrode respectively. In the same way, substituting equation (8) and equation (9) into equation (3), the mean ion concentration is given by

$$N_i = \frac{I_i \ln(r_2/r_1)}{2\pi LZ_i eV} \tag{10}$$

The obstruction of the flow caused by the wire electrode was neglected due to the very thin ($r_1 << r_2$) wire electrode. The mean residence time of particles in the charging zone of the corona-wire charger is equal to

$$t = \frac{\pi r_2^2 L}{Q_a} \tag{11}$$

For the standard aerosol flow of 5.0 liter/min, the mean

aerosol residence time in the charging zone is 0.074 s at atmospheric pressure.

3.3 Ion Concentration at Charger Outlet

From the ionic current at the charger outlet, the ion number concentration, N_i, can be calculated from the expression

$$N_i = \frac{I}{eQ} \tag{12}$$

where I is the ionic current, e is the elementary charge and Q is the volumetric air flow through the filter. The ionic current measurements were translated into ion number concentrations given the total air flow rate through the charger. The ionic concentration was then used as an input for the charging models.

3.4 Electric Field inside the Charger

A numerical model was developed to investigate flow and electric fields in the charging zone of the charger to give a better understanding on the operating of the chargers. The model is consists of two parts; flow field and electric field modeling. For electrostatic field modeling, the Poisson's equation for the electric potential can be used. However, the space-charge effect on the electric field can be neglected (ρ = 0) for low aerosol concentration, typically less than 10^{12} particles/m^3, and with low particle charge level [5, 6]. For the present charger configurations, the resulting Laplace's equation in the 2-D, axisymmetric, cylindrical coordinates is given as follows:

$$\frac{1}{r}\frac{\partial}{\partial r}\left(r\frac{\partial V}{\partial r}\right)+\frac{\partial^2 V}{\partial z^2}=0 \tag{13}$$

Once the electric potential is obtained, the electric field strength in the r- and z- directions can be calculated by the following equations

$$E_r = -\frac{\partial V}{\partial r}, \qquad E_z = -\frac{\partial V}{\partial z} \tag{14}$$

In the simplified geometry, the electric field strength are expressed by

$$E_r(r,z) = E_r(r) = -\frac{V}{r\ln(r_2/r_1)}, \tag{15}$$

$$E_z(r,z) = 0 \tag{16}$$

For the boundary conditions used, constant potentials are applied to the corona-electrode (V = corona voltage), the outer electrode (V = 0), and the zero gradient conditions is applied to the boundaries with out walls.

3.5 Flow Field inside the Charger

Flow conditions inside the charger were assumed to be steady, incompressible and laminar. Based on the principle of momentum conservation, the incompressible Navier-Stokes equations can be applied in this case. In these axisymmetric geometries, the continuity and Navier-Stokes equations used in this model can be written in the 2-D cylindrical coordinates as follows.

Continuity equation:

$$\frac{1}{r}\frac{\partial}{\partial r}(ru_r)+\frac{\partial}{\partial_z}(u_z)=0 \tag{17}$$

Navier-Stokes equations:
For the radial component (in r-direction),

$$\begin{aligned} u_r\frac{\partial u_r}{\partial r}+u_z\frac{\partial u_r}{\partial z}-\frac{u_\theta^2}{r} &= -\frac{1}{\rho}\frac{\partial p}{\partial r} \\ +\mu\left(\frac{\partial}{\partial r}\left(\frac{1}{r}\frac{\partial}{\partial r}(ru_r)\right)+\frac{\partial^2 u_r}{\partial z^2}\right)-\mu\frac{1}{r^2}u_r & \end{aligned} \tag{18}$$

For the axial component (in z-direction),

$$u_r\frac{\partial u_r}{\partial r}+u_z\frac{\partial u_z}{\partial z}=-\frac{1}{\rho}\frac{\partial p}{\partial z}+\mu\left(\frac{1}{r}\frac{\partial}{\partial r}\left(r\frac{\partial u_z}{\partial r}\right)+\frac{\partial^2 u_z}{\partial z^2}\right) \tag{19}$$

For the circumferential component (in θ-direction)

$$u_r\frac{\partial u_\theta}{\partial r}+u_z\frac{\partial u_\theta}{\partial z}=\mu\left(\frac{1}{r}\frac{\partial}{\partial r}\left(r\frac{\partial u_\theta}{\partial r}\right)+\frac{\partial^2 u_\theta}{\partial z^2}\right)-\frac{2\mu}{r}\left(\frac{\partial u_\theta}{\partial r}\right) \tag{20}$$

where u_r is the velocity component in the r-direction, u_z is the velocity component in the z-direction, u_θ is the velocity component in the θ-direction, p is the pressure and μ is the kinematic viscosity of air. For the boundary conditions used, no slip boundary was applied to all the solid walls included in the computation domain, and fixed velocity boundary condition was applied to the aerosol inlet. The velocity at inlet was calculated from the flow rate through the charger. Uniform velocity profile was assumed at the sheath and aerosol inlet across the cross

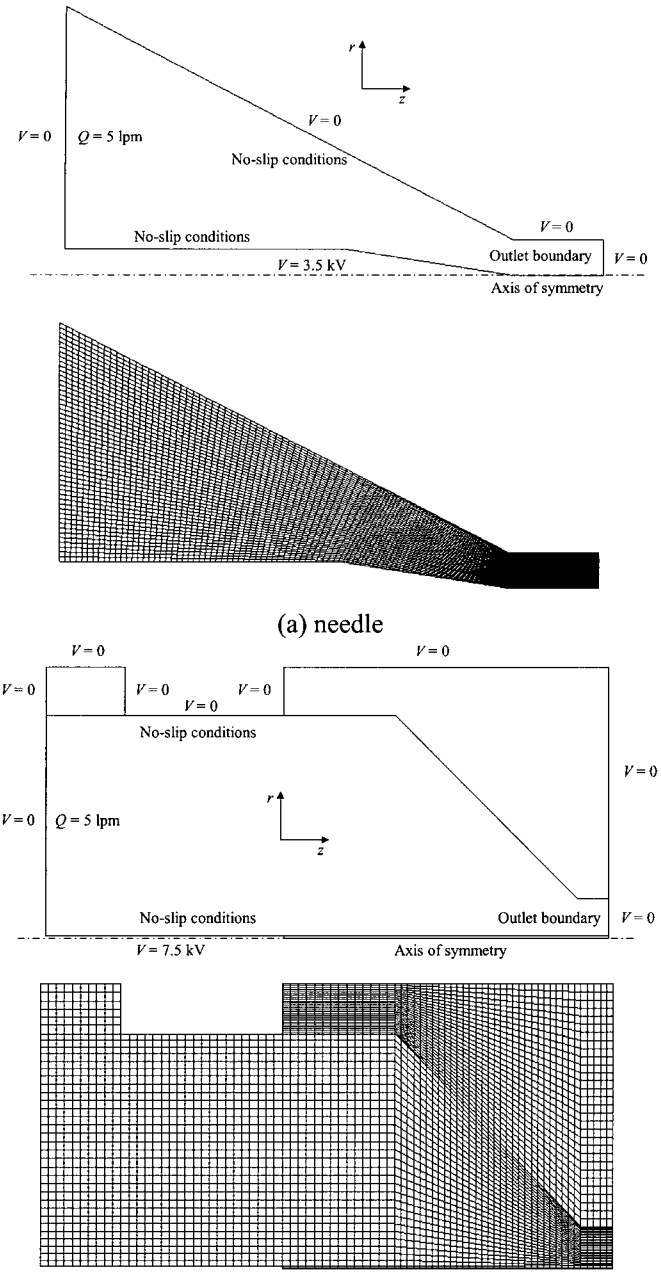

Fig. 3 Numerical domains of the needle and wire-cylinder chargers

section of the inlet tubes. Numerical computation was performed using a commercial computational fluid dynamic software package, CFDRC^{TM}. The solution domain was divided into a number of cells known as control volumes. In the finite volume approach of CFDRC^{TM}, the governing equations were numerically integrated over each of these computational cells or control volumes. Fig. 3 shows physical and computational domains as well as cross sections of the computational mesh distribution in the charging zone for each charger. A structured grid was used. A total of about 6,000 meshes were distributed in computational domain of the corona-needle charger (Fig. 3a.), while the corona-wire charger, a mesh with 4,000 meshes was used (Fig. 3b.).

4. Results and Discussion

Fig. 4 shows current-voltage characteristic of the positive and negative coronas produced from the needle and wire-cylinder corona chargers. In the needle charger, the spark-over phenomena occurred for the positive corona voltages larger than about 5.0 kV and negative corona voltages larger than about 4.5 kV. Above these values, the current was found to exhibit a fluctuation in an uncontrollable manner and no measurement could be made

Meanwhile, the wire charger was able to operate stably at 10 kV applied voltage. However, at the same corona

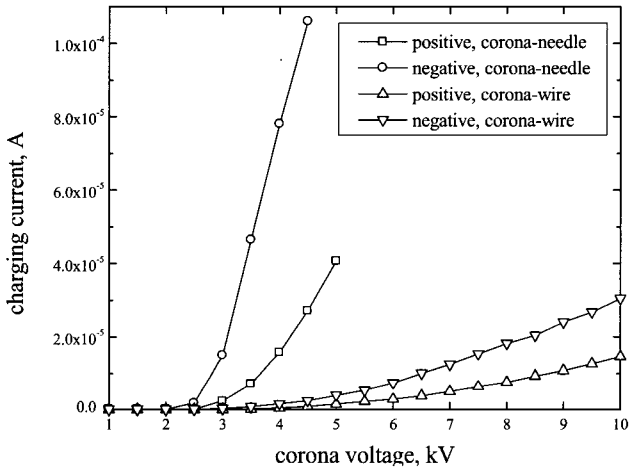

Fig. 4 Current-voltage characteristics in the charging zones of the needle and wire-cylinder chargers

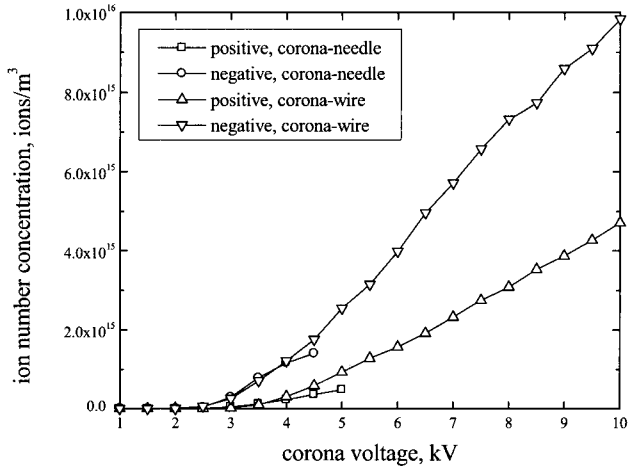

Fig. 5 Variation in ion number concentration with applied voltage inside chargers

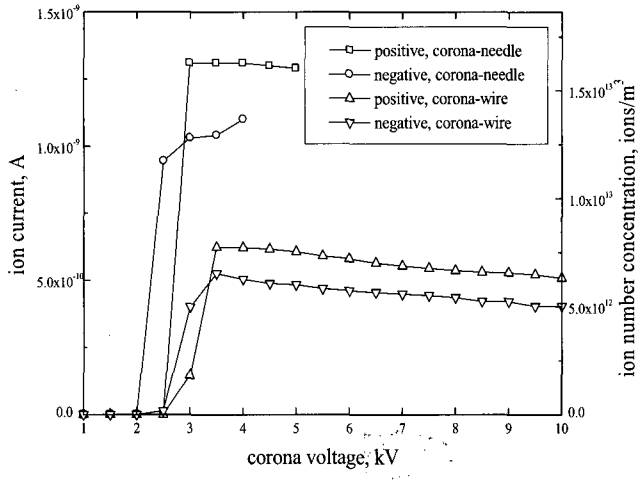

Fig. 6 Variation in ion current and concentration with applied voltage at the charger outlet

voltage, magnitude of the charging current was markedly smaller for the wire charger, compared to the needle one. Even at the maximum possible applied voltage under present setup (10 kV), the charging currents from the wire charger were approximately 3.5 and 2 times smaller than those from the needle charger just before the spark-over for the positive and negative coronas, respectively. Generally, the currents for negative ions were slightly higher than those for positive ions. This was expected because negative ions have higher electrical mobility than positive ions. A high ion concentration in the charging region of a charger is desirable for high aerosol charging efficiency. The ion concentration was approximately proportional to the ion current. This ion current increased with the electric field, hence applied voltage. This was the case for both chargers, as clearly depicted in Fig 5.

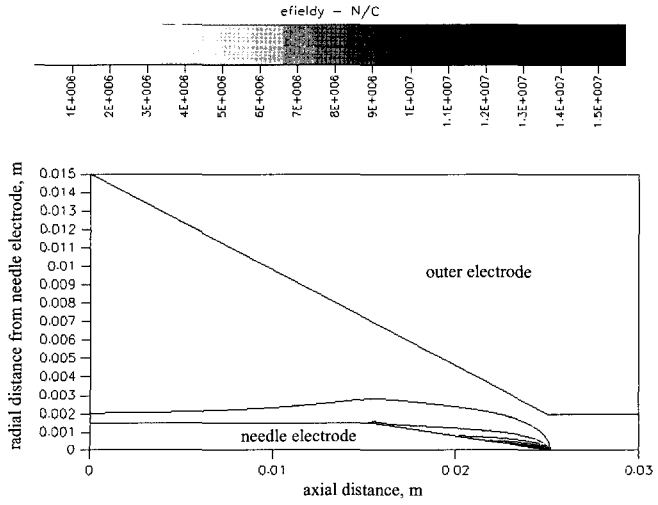

(a) needle

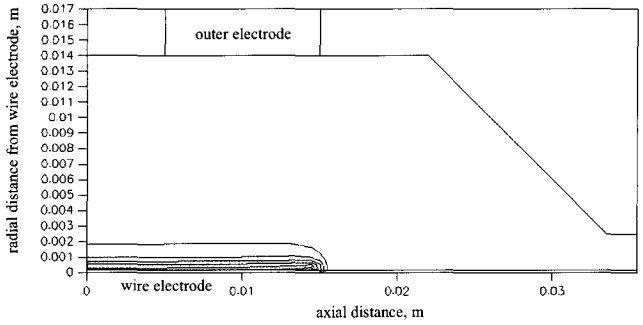

(b) wire-cylinder

Fig. 7 Distributions of electric field strength inside the needle and wire-cylinder chargers

The number concentration of the positive and negative ions leaving the corona-needle and corona-wire chargers were shown as a function of the corona voltage in Fig. 6. In the needle charger, negative corona (i.e. negative ion generation) appeared at about 2.2 kV, while a larger voltage, about 2.5 kV, was needed for the onset of positive corona. In the case of positive ions, ion concentration appeared to depend on corona voltage only within a narrow interval of voltages. For larger voltages, ion number concentration

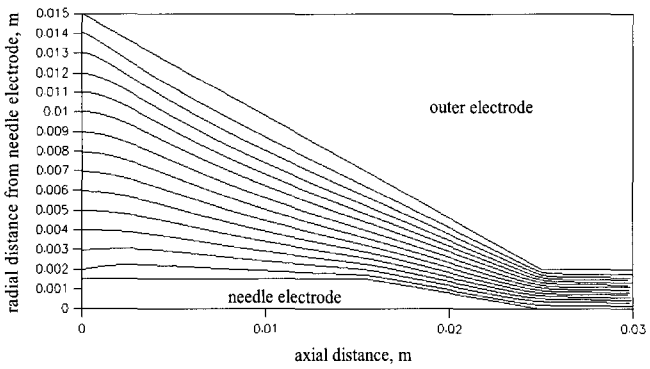

(a) needle

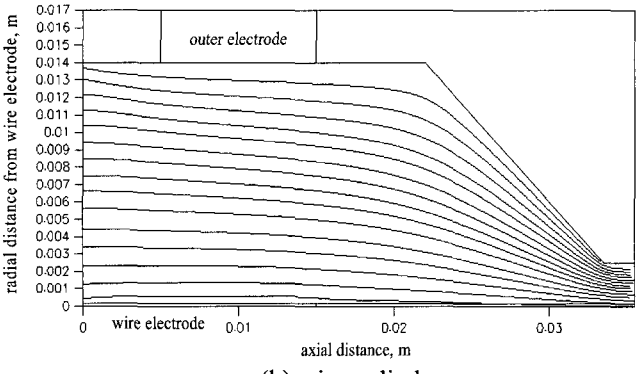

(b) wire-cylinder

Fig. 8 Particle trajectories inside the needle and wire-cylinder chargers

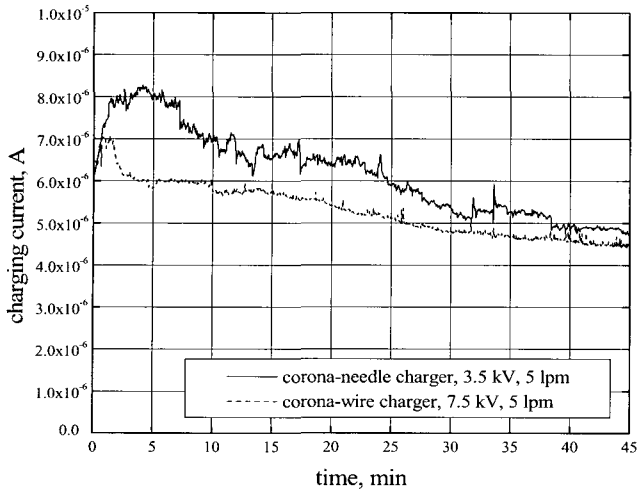

Fig. 9 Evolution of charging current for each charger with operating time

practically became a constant, independent of the applied voltage. Meanwhile, the ion concentration of negative ions increases with increasing corona voltage. For the corona-wire charger, the onset of negative corona was about 2.8 kV, and positive corona was about 3.0 kV. For both cases, ion concentrations were also found to increase with increasing corona voltage only within a narrow voltage interval. For larger voltages, ion number concentrations decreased slightly with increasing corona voltage. As it can be seen from Fig. 6, at the same corona voltage, the magnitude of the ion number concentration was markedly smaller for the wire-cylinder corona charger, compared to the needle corona charger. This was attributed to high ions loss inside the wire-cylinder charger. Nonetheless, the needle charger was found to become unstable at lower applied voltage. It was also evident that the ion number concentrations for positive corona of both charges were slightly higher than those for negative corona. This was because negative ions have higher electrical mobility than positive ions, hence they were more likely to impact and deposit on the charger's wall. When the applied voltage increased, ion number concentration and electric field strength were found to increase, inducing a better particle charging rate and more particle loss due to deposition on the electrodes and on the wall.

Examination of flow and electric fields in and around the charging regions from numerical simulation results for both chargers revealed that (Figs. 7, 8) there existed regions of strong electric field in close proximity to the tip of the needle and the wire. Flow speed in these regions was faster in case of the needle charger than that of the wire-cylinder charger. Fig. 9 illustrates the evolution of charging currents measured for both chargers operating at their corresponding stable corona voltages with time. A decrease in charging efficiency as shown by a decline of charging current with time in Fig. 7 was a direct result of evolution from a stable discharge to spark-over or arcing phenomenon. Both the needle and wire chargers similarly exhibited a continuous reduction in charging current. However, current from the needle charger was found to decline in a high rate than that from the wire-cylinder charger. The buildup of particles deposited on the wall appeared to affect the charger performance adversely.

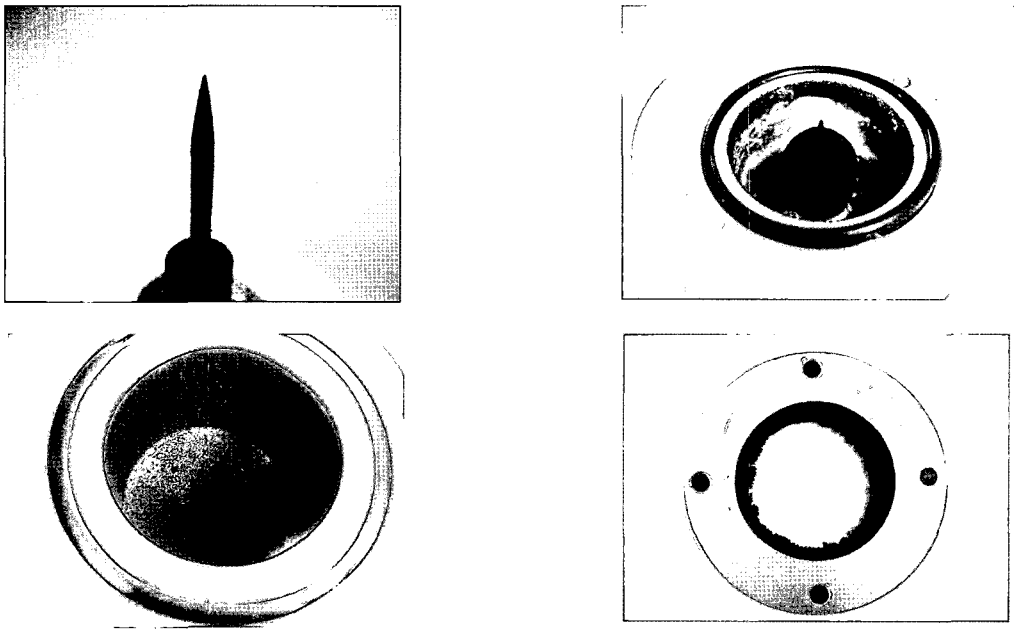

(a) needle (b) wire-cylinder

Fig. 10 Particle deposition inside the charging regions for both chargers

Particle collection on the electrodes and walls formed dendrites build-up (Fig. 10), causing a change in the needle and wire surface geometry and modifying the discharge regimes. This gave rise to a great change in the electric field around the electrodes which lessened the charging efficiency.

5. Conclusion

In this study, needle and wire-cylinder corona aerosol chargers were constructed and tested. Comparison of both chargers' performance based on their electrical discharge characteristics and operation was carried out and discussed. A semi-empirical method, based on current measurements, was used to calculate average ion concentration in the charging zone and at the outlet for each charger. Additionally, a numerical model was developed to investigate flow and electric field patterns in the charging zone for each charger to give a better understanding on the operation. Non-uniform distributions of electric field strength and high speed flow were identified. Charging current and ion number concentration as a function of corona voltage were evaluated. Effect of particle deposition on the corona electrodes and on the grounded cylinder was presented. The charging current and ion concentration in the charging zone were found to increase with corona voltage for each charger. Ion as well as particle losses inside both chargers increased with applied voltage. Results from ion current measurement at the outlet of both chargers revealed that ion loss within the wire-cylinder charger was higher than the needle charger. Particle deposited on the corona electrodes and the grounded cylinder for each charger also increased with operating time.

Acknowledgements

Financial support from the National Electronic and Computer Technology Center (NECTEC), National Science and Technology Development Agency (project no. NT-B-22-E7-11-47-12) is gratefully acknowledged.

References

[1] L. Unger, D. Boulaud, and J. P. Borra, "Unipolar field charging of particles by electric discharge: effect of particle shape," *Journal of Aerosol Science*, vol. 35, pp. 965-979, 2004.

[2] A. Hernandez-Sierra, F. J. Alguacil, and M. Alonso, "Unipolar charging of nanometer aerosol particle in a corona ionizer," *Journal of Aerosol Science*, vol. 34, pp. 733-745, 2003.

[3] P. Intra and N. Tippayawong, "Approach to characterization of a diode type corona charger for aerosol size measurement," *KIEE International Transactions on Electrophysics & Applications*, vol. 5-C, pp. 196-203, 2005.

[4] J. Keskinen, K. Pietarinen, and M. Lehtimaki, "Electrical low pressure impactor," *Journal of Aerosol Science*, vol. 23, pp. 353-360, 1992.

[5] D. R. Chen and D. Y. H. Pui, "Numerical modeling of the performance of differential mobility analyzers for nanometer aerosol measurement," *Journal of Aerosol Science*, vol. 28, pp. 985-1004, 1997.

[6] R. P. Camata, H. A. Atwater, and R. C. Flagan, "Space-charge effects in nanoparticle processing using the differential mobility analyzer," *Journal of Aerosol Science*, vol. 32, pp. 583-599, 2001.

Panich Intra
He received BS.Tech.Ed. degree in electrical engineering from Rajamangala Lanna University of Technology in 2001 and M.Eng. degree in energy engineering from Chiang Mai University in 2003. He recently graduated with Ph.D. in mechanical engineering at Chiang Mai University. His interests include electro-aerosol measurement technology, automation control and instrumentation.

Nakorn Tippayawong
He received B.Eng. and Ph.D. degrees in mechanical engineering from Imperial College, UK in 1996 and in 2000, respectively. He is currently an assistant professor at Chiang Mai University. His research interests are HV applications in aerosol system, renewable energy.